Journal of ELECTRONIC MATERIALS, Vol. 48, No. 8, 2019
https://doi.org/10.1007/s11664-019-07333-0
© 2019 The Author(s)

On Investigations of the Optical Absorption Coefficient of Gold and Germanium Implanted Silicon with the Use of the Non-destructive Contactless Photo Thermal Infrared Radiometry

Ł. CHROBAK[1,2] and M. MALIŃSKI[1]

1.—Faculty of Electronics and Computer Science, Koszalin University of Technology, 2 Śniadeckich St., 75-453 Koszalin, Poland. 2.—e-mail: lukasz.chrobak@tu.koszalin.pl

In this paper results of investigations of Au^{2+} and Ge^{+} ion-implanted silicon samples with the use of the nondestructive frequency and the space domain photo thermal infrared radiometry (PTR) method are presented. Frequency amplitude characteristics and spatial amplitude distributions of the PTR signal for the implanted silicon samples were measured and analyzed. Measurements have been performed for several wavelengths of the exciting light. The dependence of the amplitude of the PTR signal on the optical and recombination parameters of the implanted layers has been analyzed experimentally and theoretically and discussed. The objective of this work is to present the possibilities of investigations of the influence of the high energy and high dose implantation process into silicon on the optical and recombination parameters of implanted silicon with the use of the frequency and spatial domain PTR method. Observed changes in the measured signal have been explained by simultaneous changes of values of the optical absorption coefficient and carriers lifetime of implanted layers.

Key words: Ion implanted silicon, nondestructive optical characterization, optical absorption coefficient, photo thermal infrared radiometry technique, implanted areas imaging

INTRODUCTION

Ion implantation causes changes in optical and recombination parameters of semiconductors and has a wide range of applications in a modern optoelectronics. For example, it enables making structures of a very large scale of integration.[1,2] Au is one of the most important impurities in semiconductors, which allows controlling of the minority carriers lifetime, e.g., in fast switching devices.[3,4] Implantation of Au ions allows obtaining strictly predictable structures. Its importance in designing of the functional silicon nanostructures has been described in paper.[5] Gold ion implantation also can be used in a production of embedded Si nanocrystals.[6] $Si_{1-x}Ge_x$ mixed crystals are used to improve the parameters of both CMOS and heterojunction bipolar transistors. To synthesize $Si_{1-x}Ge_x$ mixes crystals Ge^{+} ion implantation is used.[7,8] This implanation creates, however, both interstitial-type and vacancy-type defects in silicon.[9] At present $Si_{1-x}Ge_x$ mixed crystals have been applied in the modern technology of electronic devices.[10] The issue of oxidation of silicon structures implanted with germanium ions is presented in paper.[11] In the last years nondestructive methods still have a wide range of applications in investigations of different types of materials.[12] In this work we report results of investigations of Au^{2+} and Ge^{+} ion-implanted silicon with the Photo Thermal Infrared Radiometry (PTR) method.[13] This method is used for investigations of semiconductor materials like other photoacoustic (PA),[14–20] photopyroelectric[21–23] and Modulated Free Carriers Absorption (MFCA)[24–28]

(Received February 21, 2019; accepted May 29, 2019; published online June 11, 2019)

methods. The PTR method has a wide range of different applications in investigations of many types of materials. One of the first and the most important ones is its application for investigations of so called transport properties of Si wafers.[29] The PTR method was also used for investigations of implanted Si samples. Results of investigations of B implanted Si samples are presented in.[30] Results of the PTR investigations of silicon implanted with P are presented in.[31,32]

Determination of the thermal diffusivity of different metals, such as: stainless steel, nickel, titanium, tungsten, molybdenum, zinc, and iron has been described in.[33] Investigations of the thermal interface conductance and the mechanical adhesion strength in Cu-coated glassy carbon was reported in.[34] The heat transport in copper–carbon flat model systems was studied by the frequency-dependent photothermal radiometry and was described in.[35] The PTR method was used for monitoring of amorfization of the implanted layers in silicon.[36,37] The results of investigations of thin films with the use of the infrared radiometry have been presented in papers.[38,39] The possibility of determination of thermal parameters of silicon and silicon–germanium crystals has been analyzed and described in.[40] The PTR method also turned out to be a good tool for the thickness control of coatings.[41] The photothermal radiometry can be used in the pulsed or periodic mode.[42] In this paper the applications of the PTR method in the frequency and spatial modes have been presented.

EXPERIMENTAL SET-UP AND A THEORETICAL BACKGROUND

The experimental set-up for the frequency and spatial PTR measurements of semiconductor wafers has been presented in Fig. 1.

Silicon samples were illuminated with the laser light of diodes emitting at 808 nm, 660 nm, 520 nm, and 480 nm. The optical power of the lasers was 200 mW. The intensity of the illuminating light was modulated by the LDC205C Benchtop LD Current Driver. As a result of the illumination periodical thermal and plasma waves were generated in the samples. The driver was controlled by a TTL signal of the SR 830 lock-in amplifier. The periodical component of the thermal radiation of the samples was detected by the infrared photovoltaic detector PVI-3TE-5 produced by the VIGO System S.A. The spectral sensitivity range of this photovoltaic detector is optimized for the 5.5 μm. This detector is equipped with a transimpedance amplifier for the frequency range (10 Hz–1 MHz) and cooled with the thermoelectric system. The construction of a X–Y table is based on MLA-K modules. They are driven by step motors. All measurements were performed at room temperature and were computer controlled. The signal from a photovoltaic detector was acquired with a SR 830 Stanford Research phase

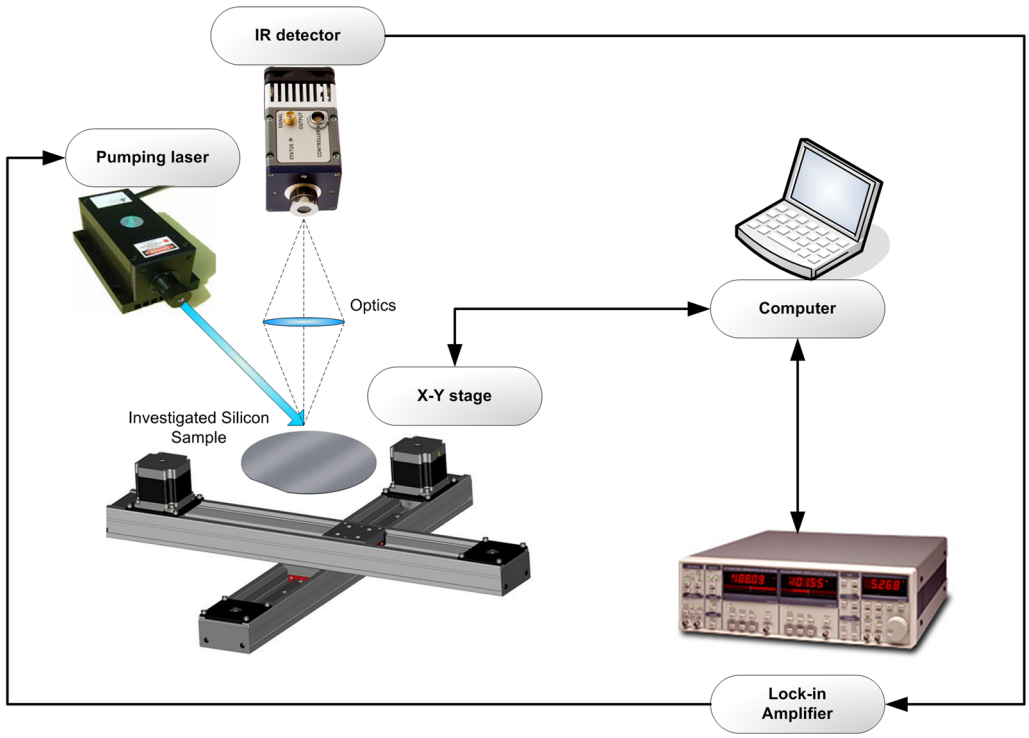

Fig. 1. Schematic diagram of the experimental set-up used in the PTR measurements.

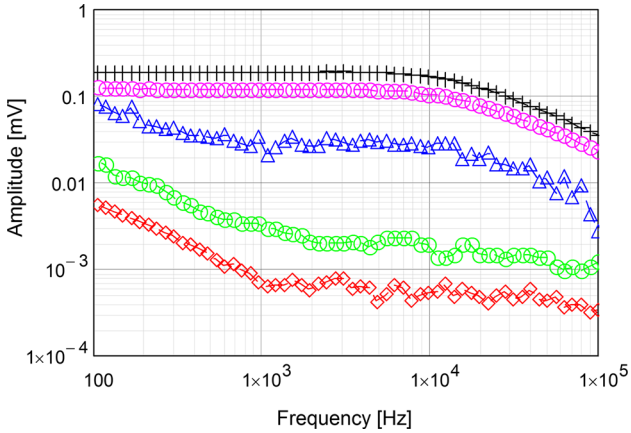

Fig. 2. Experimental amplitude PTR frequency characteristics of Ge^+ ion implanted Si samples measured at different wavelengths of the exciting laser light. Pluses-nonimplanted area of the sample λex = 808 nm, diamonds-implanted area λex = 480 nm, circles-implanted area λex = 520 nm, triangles-implanted area λex = 660 nm, circles-implanted area λex = 808 nm.

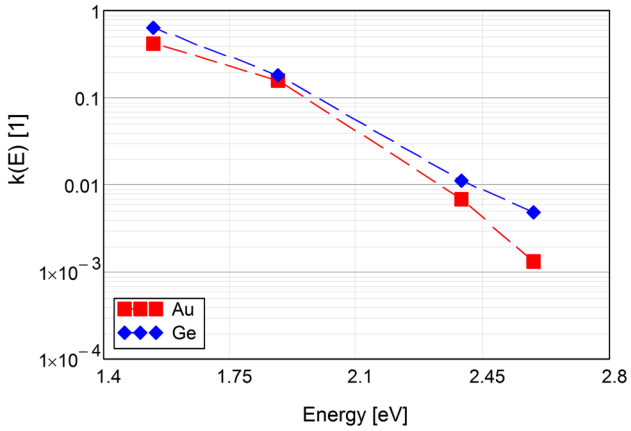

Fig. 3. Experimental amplitude dependence $k(E)$ of the PTR amplitude signals on the energy of absorbed photons measured for silicon samples implanted with Au^{2+} and Ge^+ ions. The frequency of modulation of the intensity of the exciting light f = 1 kHz.

sensitive amplifier which measured the amplitude and phase of the PTR signal.

The general expression for the PTR signal of a one-layer sample is expressed by formula (1) described in papers.[43,44] It is a sum of the thermal and plasma wave components.

$$S_{\mathrm{PTR}}(f) = a \cdot \int_0^l \Delta T(x,f) \cdot \partial x + b \cdot \int_0^l \Delta N(x,f) \cdot \partial x, \tag{1}$$

where x is a spatial coordinate, f—frequency of modulation, ΔT—is a periodical component of the temperature, ΔN—is a periodical component of the concentration of excess carriers, l—is the thickness of the sample.

The general expression for the PTR signal in a case of a two-layer sample is a sum of the PTR signals from the layer and from the substrate. The PTR signal can be then expressed by formula (2) and is described in detail in paper.[45]

$$\begin{aligned} S_{\mathrm{PTR}} = {} & a_i \int_0^d \Delta T_i(x,f) + b_i \int_0^d \Delta N_i(x,f) \\ & + a_s \int_d^l \Delta T_s(x,f) + b_s \int_d^l \Delta N_s(x,f), \end{aligned} \tag{2}$$

where d—is the thickness of the first, upper layer, l—is the thickness of the substrate.

For the frequencies of modulation bigger than f = 1 kHz the plasma components dominate in the PTR signal and the PTR signal can be reduced to formula (3).

$$S_{\mathrm{PTR}} = b_i \int_0^d \Delta N_i(x,f) + b_s \int_d^l \Delta N_s(x,f) \tag{3}$$

In this paper formula (4) for the PTR signal of the implanted layer and the substrate was used. It is correct for the frequencies of modulation when the plasma wave component dominates in the PTR signal. In practice, for the investigated samples, it was for the frequencies above f = 1 kHz.

$$\begin{aligned} S_{\mathrm{PTR}} = {} & I_0 \left[b \int_0^d \Delta N_i(x,f,\tau_i,D_i,\beta_i(E)) \right] \\ & + I_0 e^{(-\beta_i(E)d)} \left[b \int_d^l \Delta N_s(x,f,\tau_s,D_s,\beta_s(E)) \right], \end{aligned} \tag{4}$$

where f is the frequency of modulation of the intensity of the beam of light, d is the thickness of the implanted layer, l—is the thickness of the substrate, $D_{i,s}$ is the diffusion coefficient of carriers, $\beta_{i,s}$ (E) is the optical absorption coefficient of the semiconductor for the energy of photons E of the illuminating beam of light, $\tau_{i,s}$ is the lifetime of excess carriers. Symbols i and s denote the implanted layer and the substrate respectively.

EXPERIMENTAL RESULTS

P-type silicon wafers (111) grown by the Czohralski method were investigated. A dopant concentration in the investigated samples was about 10^{15} cm^{-3}. Resistivity of the samples was 10 Ω cm. Parameters of the implantation with Au^{2+} and Ge^+ ions: energy of ions 200 keV and 100 keV respectively, a dose of implantation was 10^{14} cm^{-2}. For the implantation a focused ion beam (FIB) machine

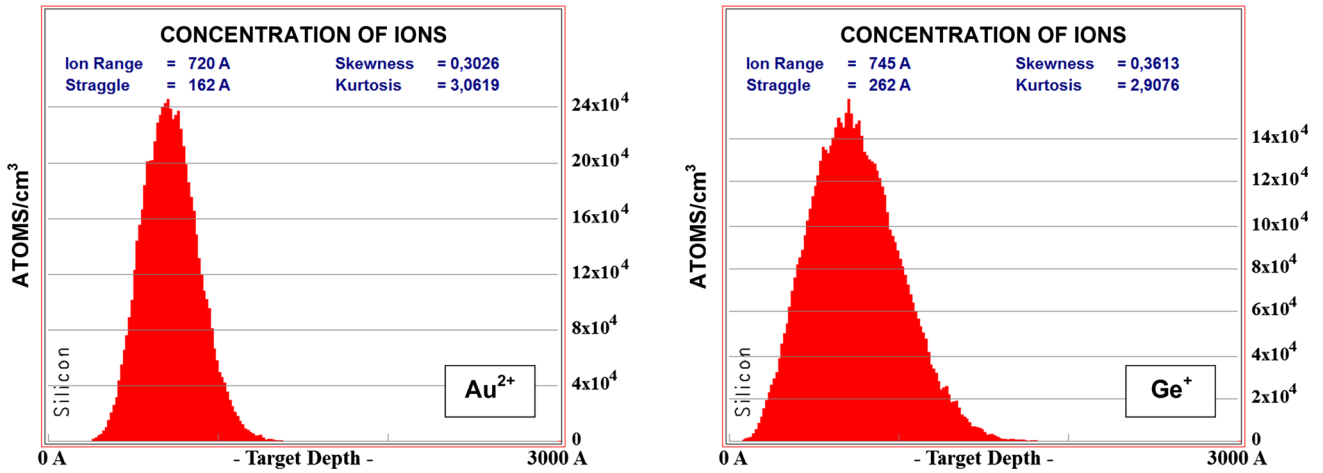

Fig. 4. Concentration of Au^{2+} and Ge^{+} ions in silicon computed in the TRIM software. The thickness of the Au^{2+} implanted layer is d = 1440 A. The thickness of Ge^{+} implanted layer is d = 1490 A.

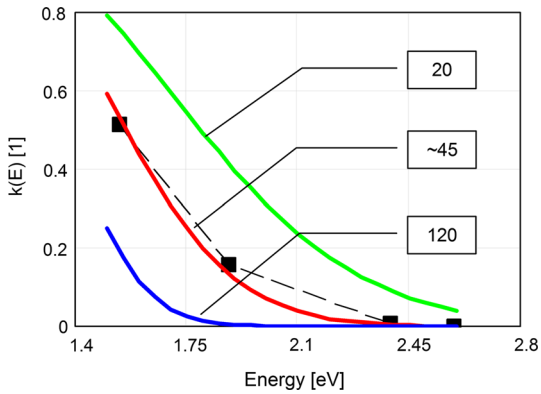

Fig. 5. Theoretical and experimental dependences of the $k(E)$ function on the energy of photons for the Au^{2+} implanted silicon layer. Squares are experimental $k(E)$ results. Solid lines are theoretical characteristics computed for different values of n. The best fitting of the theoretical characteristics to experimental data for the Au^{2+} implanted silicon layer was obtained for the value of the parameter n = 45.49 ± 6.20.

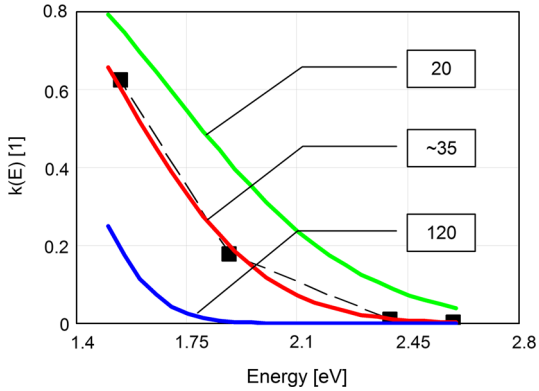

Fig. 6. Theoretical and experimental dependences of the $k(E)$ function on the energy of photons for Ge^{+} implanted silicon layer. Squares are experimental $k(E)$ results. Solid lines are theoretical characteristics computed for different values of n. The best fitting of the theoretical characteristics to experimental data for the Ge^{+} implanted silicon layer was obtained for the value of the parameter n = 35.30 ± 4.35.

EIKO-100 under high-vacuum conditions of 10^{-7} mBar was used. Dimensions of the implanted area were 2 mm × 2 mm. Dimensions of the silicon substrate were 5 mm × 5 mm × 0.375 mm.

The experimental amplitude PTR frequency characteristics at different wavelengths of the excitation light, obtained in the measurements of the investigated Ge^{+} ion implanted samples are presented in Fig. 2.

The dependence $k(E)$, which is analyzed in this paper, is defined as the ratio of the amplitude of the PTR signal when the implanted region of the sample is illuminated to the amplitude of the PTR signal when the not implanted region of the silicon sample is illuminated. The frequency of modulation is above 1 kHz and below 10 kHz, where the plasma contribution to the PTR signal dominates.

The experimental characteristics $k(E)$ were determined for each wavelength of the illuminating light for both ions and the frequency f = 1 kHz. They were determined from the frequency characteristics of the amplitude of the PTR signal.

The experimental characteristics $k(E)$, as a function of the energy of photons of the illuminating light, for investigated Au^{2+} and Ge^{+} implanted silicon samples, are presented in Fig. 3.

To determine the average optical absorption coefficient spectrum $\beta_{imp}(E)$ of the implanted layer, its thickness must be known.

The TRIM application has been used for the estimation of the thickness of implanted layers. Results of these calculations have been presented in Fig. 4.

Let us assume that the average optical absorption coefficient spectrum of the implanted layer is n times bigger than the optical absorption coefficient spectrum of the substrate. Assuming that the lifetime of carriers in the implanted layer is at least hundreds of time smaller than the lifetime of

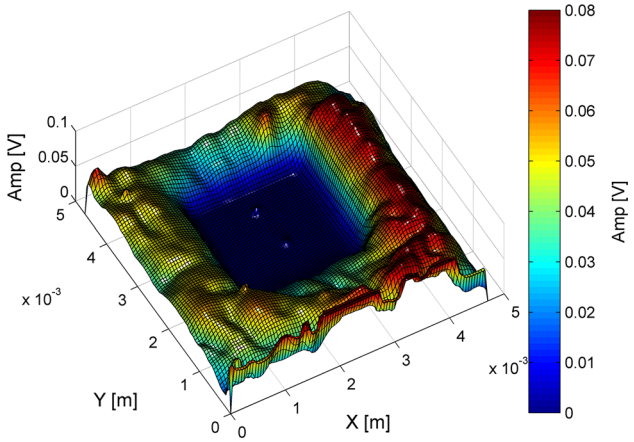

Fig. 7. The amplitude spatial distribution of the PTR signal for the example Au^{2+} implanted silicon sample for λ_{ex} = 480 nm and f = 1 kHz.

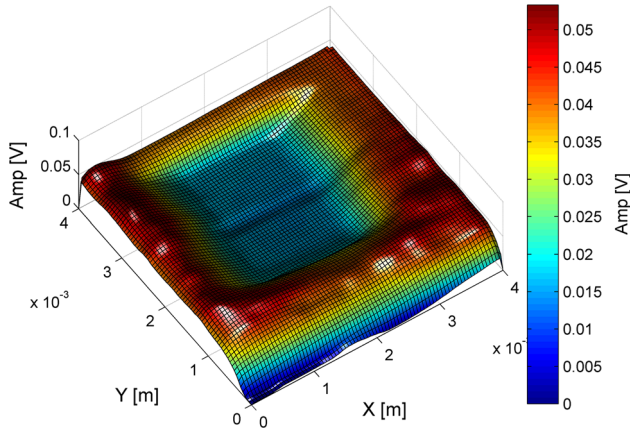

Fig. 8. The amplitude spatial distribution of the PTR signal for the example Ge^{+} implanted silicon sample for λex = 808 nm and f = 1 kHz.

carriers in a nonimplanted silicon, it can be proved that from the following formula (4) the dependence $k(E)$ can be expressed, in the first approximation, as:

$$k(E) = \exp[-n \cdot \beta_s(E) \cdot d], \tag{5}$$

where E is the energy of photons, d is a thickness of the implanted layer, $\beta_s(E)$ is the optical absorption coefficient spectrum of the substrate, n is the number.

The characteristics of the $k(E)$ dependence on the energy of absorbed photons, both theoretical and experimental, for the Au^{2+} implanted silicon are presented in Fig. 5.

The characteristics of the $k(E)$ dependence on the energy of absorbed photons, both theoretical and experimental, for the Ge^{+} implanted silicon are presented in Fig. 6.

The spatial distribution of the amplitude of the PTR signal obtained for the investigated Au^{2+} implanted silicon sample is presented in Fig. 7.

The spatial distribution of the amplitude of the PTR signal obtained for the investigated Ge^{+} implanted silicon sample is presented in Fig. 8.

From the results presented in Figs. 7 and 8 a strong drop of the amplitudes of the PTR signal coming from the implanted areas is well visible for both Au^{2+} and Ge^{+}.

Presented experimental characteristics of the implanted areas in silicon carry information about changes of the optical and recombination parameters of implanted regions.

CONCLUSIONS

In this paper results of investigations of the Au^{2+} and Ge^{+} implanted silicon samples with the use of the frequency and space domain photo thermal infrared radiometry method have been presented. For the samples implanted with Au^{2+} and Ge^{+} ions, of the energy 200 keV and 100 keV, respectively, and a dose 10^{14} cm^{-2}, a considerable drop of the amplitude of the PTR signal was observed for the frequencies of modulation above f = 1 kHz and below 10 kHz. This is the frequency region where the plasma component dominates in the PTR signal. This decrease, expressed by a characteristics $k(E)$, depended on the energy of photons of the exiting laser light. It decreased with the increase of the energy of photons and its character was very similar for investigated ions. The thickness of the implanted layers, computed in a TRIM program, was also similar (1440 A and 1490 A). Taking into account the thickness of the implanted layers and the values of their $k(E)$ functions, their average optical absorption coefficient spectra were computed. Comparison of the optical absorption coefficient spectrum of a non implanted silicon and the optical absorption coefficient spectra of Au^{2+} and Ge^{+} implanted silicon layers leads to the conclusion that they increased about 45 and 35 times, respectively. The lifetime of carriers in the implanted areas decreased about 10^4 times, under the assumption that the value of a diffusion coefficient of carriers of the implanted area is equal to $D_i = 1.5 \cdot 10^{-4}$ cm^2/s, respective to the lifetime of carriers in the silicon substrate. The presented results also prove that the PTR method, similar to the Modulated Free Carrier Absorption method (MFCA), is very attractive from the point of view of the possibility of a visualization of the silicon after the implantation process. The spatial contrast of the PTR amplitude signal depends on the experimental parameters such as the wavelength of the illuminating light and the frequency of its intensity modulation. It can reach the maximum value close to 100% for the wavelengths of the exciting laser light λex = 480 nm and the frequency of modulation higher than f = 1 kHz. It is worth emphasizing that such a huge decrease of the amplitude of the PTR signal from the implanted areas can be explained only when the strong increase of the optical absorption coefficient and the strong decrease of the lifetime of carriers in the implanted areas are

considered simultaneously. Changes of these parameters are connected with the amorphization of implanted silicon and are the consequence of creation of structural defects, in a crystal lattice of silicon, being the result of a high energy and high dose implantation. It also turned out that because the image contrast in the amplitude spatial distribution of the PTR signal can reach, depending on the experimental parameters values, 100% then the PTR method is a perfect tool for the visualization of the implanted areas in silicon. For comparison, the optical image contrast measured for the investigated samples reached the value 10%. It was the result of the change of the optical reflection coefficient of implanted layers respective to the non implanted regions of silicon.

ACKNOWLEDGMENTS

We thank Dr. Nadezhda Kukharchyk for preparation of the silicon implanted samples.

OPEN ACCESS

This article is distributed under the terms of the Creative Commons Attribution 4.0 International License (http://creativecommons.org/licenses/by/4.0/), which permits unrestricted use, distribution, and reproduction in any medium, provided you give appropriate credit to the original author(s) and the source, provide a link to the Creative Commons license, and indicate if changes were made.

REFERENCES

1. A.G. Lewis, R.A. Martin, T.-Y. Huang, J.Y. Chen, and M. Koyanagi, *IEEE Trans. Electron. Dev.* ED-34, 2156 (1987).
2. N.W. Cheung, C.L. Liang, B.K. Liew, R.H. Mutikainen, and H. Wong, *Nucl. Instrum. Methods B* 37–38, 941 (1989).
3. J. Wong-Leung, J.S. Williams, and E. Nygren, *Nucl. Instrum. Methods B* 106, 424 (1995).
4. S. Coffa, L. Calcagno, G. Ferla, and S.U. Campisano, *J. Appl. Phys.* 68, 1601 (1990).
5. V. Lavrentiev, J. Vacik, V. Vorlicek, and V. Vosecek, *Phys. Status Solidi B* 247, 2022 (2010).
6. G. Sahu, R. Kumar, and D.P. Mahapatra, *Silicon* 6, 65 (2016).
7. M. Voelskow, I. Stoimenos, L. Rebohle, and W. Skorupa, *Phys. Status Solidi C* 8, 960 (2011).
8. K. Gao, S. Prucnal, A. Mücklich, W. Skorupa, and S. Zhou, *Acta Phys. Pol. A* 123, 858 (2013).
9. R. Kögler, A. Peeva, A. Mücklich, F. Eichhorn, and W. Skorupa, *Appl. Phys. Lett.* 88, 101918 (2006).
10. M.L. Lee and E.A. Fitzgerald, *J. Appl. Phys.* 97, 011101 (2005).
11. S.N. Dedyulin and L.V. Goncharova, *Nucl. Instrum. Methods B* 272, 334 (2012).
12. D. Balageas, X. Maldague, D. Burleigh, V.P. Vavilov, B. Oswald-Tranta, J.-M. Roche, C. Pradere, and G.M. Carlomagno, *J. Nondestruct. Eval.* 35, 18 (2016).
13. P.-E. Nordal and S.O. Kanstad, *Phys. Scr.* 20, 659 (1979).
14. M. Lukić, Ž. Ćojbašić, M.D. Rabasović, D.D. Markushev, and D.M. Todorović, *Int. J. Thermophys.* 38, 165 (2017).
15. D.M. Todorovic, M.D. Rabasovic, D.D. Markushev, V. Jovic, and K.T. Radulovic, *Int. J. Thermophys.* 38, 40 (2017).
16. A. Zegadi, M.A. Slifkin, M. Djamin, R.D. Tomlinson, and H. Neumann, *Solid State Commun.* 83, 587 (1992).
17. M. Maliński, Ł. Chrobak, and L. Bychto, *Solid State Commun.* 150, 424 (2010).
18. Ł. Chrobak, M. Malinski, and J. Zakrzewski, *Thermochim. Acta* 606, 84 (2015).
19. Ł. Chrobak, M. Maliński, and J. Zakrzewski, *Thermochim. Acta* 641, 79 (2016).
20. H. Benamrani, F.Z. Satour, A. Zegadi, and A. Zouaoui, *J. Lumin.* 132, 305 (2012).
21. K. Strzałkowski, *Mater. Chem. Phys.* 163, 453 (2015).
22. D. Dadarlat, M. Streza, O. Onija, C. Prejmerean, L. Silaghi-Dumitrescu, N. Cobirzan, and K. Strzałkowski, *J. Therm. Anal. Calorim.* 119, 301 (2015).
23. K. Strzałkowski, *J. Phys. D Appl. Phys.* 49, 435106 (2016).
24. S.W. Glunz and W. Warta, *J. Appl. Phys.* 77, 3243 (1995).
25. S.W. Glunz, A.B. Sproul, W. Warta, and W. Wettling, *J. Appl. Phys.* 75, 1611 (1994).
26. F. Sanii, F.P. Giles, R.J. Schwartz, and J.L. Gray, *Solid State Electron.* 35, 311 (1992).
27. M. Malinski, L. Chrobak, W. Madej, and N. Kukharchyk, *Int. J. Thermophys.* 38, 110 (2017).
28. Ł. Chrobak and M. Maliński, *Opt. Mater.* 86, 484 (2018).
29. A. Salnick, A. Mandelis, and C. Jean, *Appl. Phys. Lett.* 69, 2522 (1996).
30. M.E. Rodriguez, A. Mandelis, F. Rabago, and L. Nicolaides, *Anal. Sci.* 17, 277 (2001).
31. A. Othonos, C. Christofides, and A. Mandelis, *Appl. Phys. Lett.* 69, 821 (1996).
32. A. Othonos, A. Salnic, A. Mandelis, and C. Christofides, *Phys. Status Solidi A* 161, R13 (1997).
33. S. Pham Tu Quoc, G. Cheymol, and A. Semerok, *Rev. Sci. Instrum.* 85, 054903 (2014).
34. J. Pelzl, P. Kijamnajsuk, M. Chirtoc, N. Horny, and C. Eisenmenger-Sittner, *Int. J. Thermophys.* 36, 2475 (2015).
35. P. Kijamnajsuk, J. Pelzl, M. Chirtoc, N. Horny, D. Schäfer, and C. Eisenmenger-Sittner, *Int. J. Thermophys.* 33, 2132 (2012).
36. M. Maliński, M. Pawlak, Ł. Chrobak, S. Pal, and A. Ludwig, *Appl. Phys. A Mater.* 118, 1009 (2015).
37. Ł. Chrobak, M. Maliński, and M. Pawlak, *Infrared Phys. Technol.* 67, 604 (2014).
38. F. Macedo, F. Vaz, L. Rebouta, P. Carvalho, A. Haj-Daoud, K.H. Junge, J. Pelzl, and B.K. Bein, *Vacuum* 82, 1457 (2008).
39. J. Borges, F. Macedo, F.M. Couto, M.S. Rodrigues, C. Lopes, P. Pedrosa, T. Polcar, L. Marques, and F. Vaz, *Mater. Chem. Phys.* 163, 569 (2015).
40. Ł. Chrobak and M. Maliński, *Infrared Phys. Technol.* 89, 46 (2018).
41. S. Chotikaprakhan, F. Vaz, R.T. Faria Jr, A.C. Fernandes, P. Kijamnajsuk, J. Gibkes, B.K. Bein, and F. Macedo, *J. Phys: Conf. Ser.* 214, 012081 (2010).
42. A. Kusiak, J. Martan, J.L. Battaglia, and R. Daniel, *Thermochim. Acta* 556, 1 (2013).
43. A. Salnick, A. Mandelis, H. Ruda, and C. Jean, *J. Appl. Phys.* 82, 1853 (1997).
44. A. Mandelis, *Solid State Electron.* 42, 1 (1998).
45. M. Nestoros, Y. Karmiotis, and C. Christofidesa, *J. Appl. Phys.* 82, 6220 (1997).

Publisher's Note Springer Nature remains neutral with regard to jurisdictional claims in published maps and institutional affiliations.